Calorimetric and Dielectric Studies of Phase Transitions in Rubidium Nitrite†

Keiichi MORIYA,†† Takasuke MATSUO, and Hiroshi SUGA*
Department of Chemistry and Chemical Thermodynamics Laboratory, Faculty of Science, Osaka University, Toyonaka, Osaka 560
(Received December 11, 1987)

The heat capacities of $RbNO_2$ crystal have been measured between 15 and 330 K. Two phase transitions were found at (264.04±0.06) K and (83.8±0.2) K. The enthalpy and entropy of transition are (9310±450) J mol^{-1} and (35.9±1.8) J K^{-1} mol^{-1} for the former and (48±5) J mol^{-1} and (0.58±0.05) J K^{-1} mol^{-1} for the latter. The entropy of the high temperature transition was interpreted in terms of the orientational disorder of the NO_2^- ion. The dielectric constant increased from 6 to 10 as the transition temperature 264.04 K was traversed from below, indicating the increased motional freedom of the polar anion in the high temperature phase.

A variety of phase transitions arising from orientational disordering of NO_2^- ions has been found in ANO_2 type compounds, where A represents an alkali metal or monovalent thallium.[1-7]

Rubidium nitrite crystallizes in the sodium chloride structure (space group O_h^5-Fm3m).[8] The NO_2^- ions having the C_{2v} symmetry must be orientationally disordered to be compatible with the octahedral symmetry of the anion site in the lattice. Occurrence of a phase transition is expected at a lower temperature because of the disorder. This offers a possibility of studying an order-disorder transition due to ionic orientations in a structurally simple crystal. In fact, Richter and Pistorius reported that $RbNO_2$ transformed to a low-temperature monoclinic phase at (261±2) K.[8] We studied the phase transition by calorimetric and dielectric methods.

Experimental

Sample Preparation. Rubidium nitrite was prepared from $Ba(NO_2)_2 \cdot H_2O$ and Rb_2SO_4(Merck Co., Ltd., suprapur reagent) in aqueous solution. The $Ba(NO_2)_2 \cdot H_2O$ crystal was prepared from extra-pure reagents of $NaNO_2$ and $BaCl_2 \cdot 2H_2O$ (both from Wako Pure Chemicals Co., Ltd.). Colorless crystals of $RbNO_2$ were obtained by slow evaporation of the filtered solution at 298 K. The crystals were purified by recrystallization from aqueous solution and washed with a small amount of ethanol. They were further purified by 30 passages of zone melting in a quartz tube. The crystals were carefully handled in nitrogen gas. Impurity ions found by atomic absorption spectra were Cs; 0.01%, Na; 0.02%, and K; 0.002%. The mass percent of the NO_2^- ion determined by the redox titration was 35% (calcd 35.0%). Nitrate ion impurity was less than 0.1% from the ratio of the Raman intensities of the internal vibrations of NO_3^- and NO_2^- ions.[9]

DTA and DSC. The enthalpy of fusion of $RbNO_2$ was determined by differential scanning calorimetry (Perkin Elmer Model DSC II). The DSC was run at the rate of 5 K min^{-1} from the room temperature to above the melting point. The temperature, enthalpy and the entropy of fusion were (693±3) K, (11.0±1.5) kJ mol^{-1} and (16±2) J K^{-1} mol^{-1}, respectively. The small entropy of fusion indicates that the ions are disordered in the solid phase.

Differential thermal analysis was made as a preliminary to the heat capacity measurement (Fig. 1). On the first cooling (Run 1), an exothermic peak appeared at 250 K. In the first heating run (Run 2), an endothermic and subsequent exothermic peaks appeared around 251 K. A second large endothermic anomaly occurred at 263 K. In the second heating run (Run 4), the two peaks around 251 K disappeared and only the endothermic peak at 263 K occurred. This result was interpreted as follows. In the pressure-temperature phase diagram of $RbNO_2$,[8] a triple point (300 bar, 261 K) was found, at which the high-temperature form I (Fm3m), the low-temperature monoclinic form II and the high-pressure form III (Pm3m) coexist. The temperature 250 K where the first endothermic peak occurred (Run 2) is close to the III-I phase boundary extrapolated to the atmospheric pressure. In the first cooling (Run 1), the sample transformed from the phase I to the metastable high-pressure phase III. It transformed exothermically to the stable monoclinic phase II on the subsequent heating and then endothermically to the stable high temperature phase I (Run 2). The hysteretic behavior thus deduced from DTA was

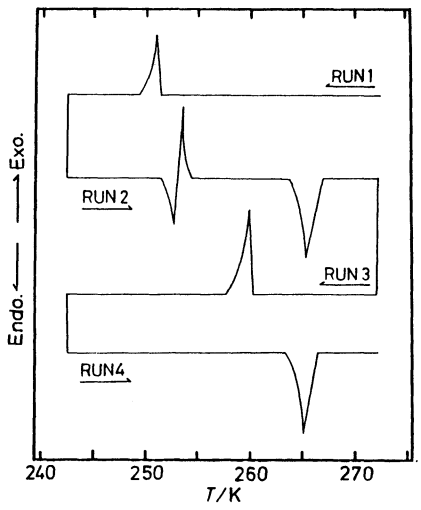

Fig. 1. DTA curves of $RbNO_2$ showing the stable–stable and metastable–stable transitions.

† Contribution No. 125 from the Chemical Thermodynamics Laboratory.

†† Present address: Department of Chemistry, Faculty of Engineering, Gifu University, Yanagido, Gifu 501-11.

Table 1. The Molar Heat Capacity of $RbNO_2$

T_{av} / K	C_p / $JK^{-1}mol^{-1}$	T_{av} / K	C_p / $JK^{-1}mol^{-1}$	T_{av} / K	C_p / $JK^{-1}mol^{-1}$	T_{av} / K	C_p / $JK^{-1}mol^{-1}$
First series		67.84	49.32	169.64	75.36	265.54	559.5
		70.16	50.55	172.55	75.77	268.14	86.09
13.26	2.691	72.53	51.86	175.45	76.22	270.92	82.91
13.78	3.220	74.92	53.54	178.32	76.63	273.45	82.80
15.26	4.047	77.41	55.03	181.48	77.09	275.98	82.70
16.76	5.145	80.03	57.17	184.02	77.54	278.62	82.77
17.84	6.045	82.66	62.24	186.84	77.93	281.37	82.82
19.01	7.138	85.35	60.30	189.65	78.34	284.19	82.79
20.09	8.153	88.16	59.59	192.52	78.83	286.99	82.83
21.08	9.065	90.99	60.09	195.45	79.23	289.85	82.94
22.03	9.966			198.39	79.66	292.76	83.08
22.91	10.91	Second series		201.28	80.20	293.33	82.93
23.84	11.76			204.16	80.56	296.31	82.94
24.71	12.66	80.64	58.16	207.02	81.08	299.14	82.95
25.58	13.49	83.59	61.36	209.86	81.56	301.96	83.07
26.45	14.40	86.14	59.96	212.69	82.05	304.91	83.04
27.38	15.33	88.72	59.65	215.50	82.61	307.87	83.28
28.44	16.37	91.57	60.30	218.30	82.95	310.86	83.23
29.56	17.51	94.67	61.08	221.15	83.54	313.90	83.37
30.41	18.31	95.15	61.20	224.06	84.02	316.93	83.43
31.14	19.16	97.71	61.80	226.95	84.56	319.94	83.57
32.22	20.31	100.57	62.50	229.82	85.13	322.96	83.72
33.49	21.65	103.46	63.43	232.68	85.58	325.97	83.78
34.75	22.91	106.36	64.09	235.53	86.18	329.96	83.77
35.97	24.19	109.28	64.81	238.35	86.66		
37.11	25.28	112.16	65.49	239.89	86.93	Fourth series	
38.24	26.42	115.07	66.08	242.58	87.71		
39.34	27.55	118.00	66.67	245.25	88.18	70.23	50.74
40.46	28.64	120.91	67.28	247.91	88.69	71.63	51.39
41.74	29.79	123.81	67.67	250.55	89.31	73.01	52.23
43.09	30.83	126.64	68.38	252.76	89.91	74.33	52.98
44.29	32.00	129.44	68.91	254.61	90.22	75.62	53.73
45.68	33.18	132.24	69.43	256.51	90.71	76.89	54.48
47.16	34.40	135.09	70.04	258.41	91.20	78.14	55.18
48.65	35.69	138.00	70.48	260.30	91.69	79.36	56.07
50.11	36.95	140.47	70.97	262.19	92.68	80.57	57.03
51.71	38.19	143.80	71.54			81.72	58.40
53.29	39.46	146.77	71.85	Third series		82.81	62.37
54.93	40.74	149.71	72.40			83.82	75.74
56.57	42.03	152.63	72.84	260.02	91.17	84.83	61.40
58.24	43.27	155.53	73.29	262.14	92.22	85.90	59.55
60.00	44.51	158.40	73.78	263.59	1451	86.97	59.18
61.83	45.72	161.25	74.10	263.99	19300	88.09	59.24
63.74	46.90	164.08	74.58	264.04	93380	89.23	59.62
65.71	48.09	166.89	74.96	264.10	14820	90.47	59.91
				264.28	4804	91.50	59.92

heeded in the following calorimetric experiment to prepare the sample in the stable form.

Heat Capacity Measurement. Heat capacities of $RbNO_2$ crystal were measured with an adiabatic calorimeter between 13 and 330 K. The calorimetric apparatus was described elsewhere.[10-13] The sample crystal was 36.947 g in mass corresponding to 0.28102 mol. The molar heat capacities are plotted in Fig. 2 and the numerical values are given in Table 1. Graphically smoothed heat capacities and derived thermodynamic functions are given in Table 2. A small heat-capacity anomaly occurred at (83.8±0.2) K. The anomaly at (264.04±0.06) K corresponds to the endothermic peak at (261±2) K found by DTA. The anomalous heat capacity appears to start to be significant far below the transition temperature. The disordering proceeded with increasing temperature until it completed discontinuously at the phase transition. No short range effect was found in the heat capacity of the high-temperature phase in contrast to the case of $NaNO_2$[1,14] where such an effect was very significant. The time required for the thermal equilibration in the calorimeter increased near the phase transition to about three days compared with fifteen minutes normally required. Such a behavior is often observed in the first-order phase transition.

Boak and Staveley measured the heat capacity of $RbNO_2$ between 83 and 483 K.[15] General temperature dependence of the present data agrees satisfactorily with theirs where the two sets of data overlap, although the absolute values are somewhat different. The small anomaly at 83.8 K has not been reported previously. However, the hysteretic behavior

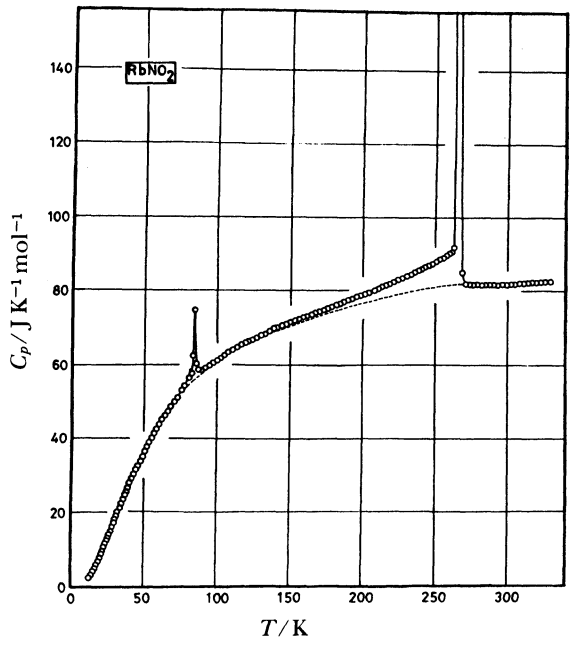

Fig. 2. Heat capacity of $RbNO_2$. The broken line represents the normal heat capacity calculated by the Debye and Einstein approximation optimized for $T \leq 65$ K.

Table 2. Thermodynamic Functions of $RbNO_2$

T	C_p°	$S^\circ - S_0^\circ$	$[H^\circ - H_0^\circ]/T$	$-[G^\circ - H_0^\circ]/T$
K	$J K^{-1} mol^{-1}$	$J K^{-1} mol^{-1}$	$J K^{-1} mol^{-1}$	$J K^{-1} mol^{-1}$
10	(1.41)	(0.45)	(0.34)	(0.11)
20	8.08	3.16	2.31	0.85
30	17.94	8.26	5.84	2.42
40	28.09	14.82	10.15	4.67
50	37.07	22.09	14.66	7.43
60	44.40	29.52	19.03	10.49
70	50.18	36.81	23.08	13.73
80	56.43	44.01	26.95	17.06
90	59.97	51.35	30.90	20.45
100	62.40	57.76	33.93	23.83
110	64.89	63.83	36.63	27.20
120	67.07	69.57	39.08	30.49
130	69.06	75.01	41.31	33.70
140	70.84	80.20	43.36	36.84
150	72.42	85.14	45.24	39.90
160	73.95	89.87	46.99	42.88
170	75.43	94.39	48.62	45.77
180	76.91	98.75	50.15	48.60
190	78.41	102.94	51.65	51.29
200	79.95	107.01	52.98	54.03
210	81.57	110.95	54.30	56.65
220	83.28	114.78	55.58	59.20
230	85.11	118.52	56.82	61.70
240	87.08	122.18	58.04	64.14
250	89.22	125.78	59.25	66.53
260	91.55	129.33	60.44	68.89
270	83.35	165.07	93.04	72.03
280	82.80	168.05	92.67	75.38
290	82.95	170.96	92.33	78.63
298.15	82.96	173.20	92.07	81.13
300	83.01	173.17	92.02	81.75
310	83.24	176.50	91.74	84.76
320	83.50	179.15	91.48	87.67

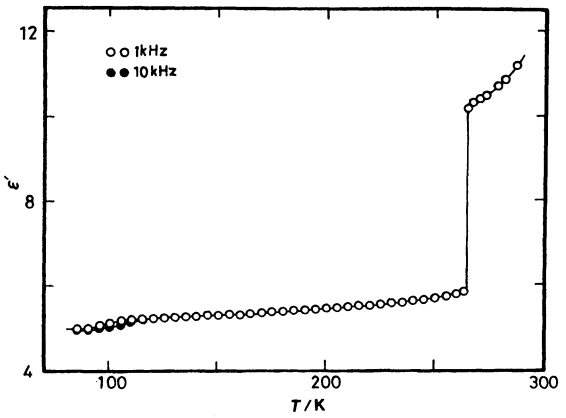

Fig. 3. Dielectric constant of $RbNO_2$ at 1 and 10 kHz.

found by the DTA has its counterpart in Boak and Staveley's calorimetric data that depended on the sample history in the corresponding temperature region. The two sets of data also agree with respect to the extended temperature range of the main anomaly below the transition temperature. The low temperature data ($T<80$ K) obtained in the present study are useful for the computation of the phonon heat capacity because the low frequency part of the entire lattice and molecular vibrational spectra is most significantly represented in the heat capacity of this temperature range.

Dielectric Constant. The dielectric constant was measured on a polycrystalline sample disc with a capacitance bridge, General Radio model 1615A, at 1 and 10 kHz. The sample was placed in a doubly thermostated environment. The temperature was regulated to 0.1 K between 80 and 290 K. As Fig. 3 shows the main transition (from phase II to I) is accompanied by a strong discontinuity of the dielectric constant characteristic of a first order phase transition. There is also a gradual increase of the dielectric constant below the transition point, corresponding to the similar gradual increase in the heat capacity.

A weak frequency dependence was found around 100 K. The magnitude of the dielectric dispersion is much smaller than those found in $TlNO_2$[2] and $CsNO_2$.[6] It is probably related to the residual disorder associated with the main transition. Because of the difference in the temperature, the dielectric dispersion and the subsidiary transition at 83 K cannot be connected with each other.

Results and Discussion

The Vibrational Heat Capacity. It is assumed that the observed heat capacity can be separated into the normal (vibrational) and the anomalous (configurational) parts. In order to evaluate the enthalpy and entropy of the phase transition, the normal heat capacity has to be estimated. $RbNO_2$ has $3\times4=12$ degrees of freedom, of which 6 degrees of freedom are the translational motion of Rb^+ and NO_2^- ions. The remaining 6 degrees of freedom are rotation (3) and internal vibrations (3) of the NO_2^- ion. The contributions from the acoustic and optical translational modes were calculated using the Debye and Einstein functions with the characteristic temperatures 108.0 and 188.3 K. The rotation vibration of the NO_2^- ion was approximated

with three independent one-dimensional vibrations of the characteristic temperature of 184.7 K. These characteristic temperatures were determined by fitting the Debye and Einstein functions to the heat capacity data between 15 and 65 K by the use of the nonlinear least squares method. There are three internal vibrations, symmetric stretching $\nu_1(A_1)$, antisymmetric stretching $\nu_2(B_2)$, and bending $\nu_3(A_1)$ modes, in the NO_2^- ion. Vibrational heat capacities of the three modes were calculated by the Einstein functions and taken into account in the least squares fitting as the known component of the total heat capacity. The vibrational frequencies, 1240 cm^{-1} (ν_1), 1320 cm^{-1} (ν_2), and 804 cm^{-1} (ν_3), were determined from the Raman and infrared spectra. The temperature dependence of the vibrational frequencies was neglected. The C_p-C_v correction becomes significant at higher temperatures. This term was calculated by the Nernst-Lindemann equation.[15]

$$C_p - C_v = A(T/T_p)C_p^2, \quad (1)$$

where $A=0.00112$ K mol J^{-1}. In this equation, T_p is the triple point temperature (approximated with the fusion temperature). The normal heat capacity was thus calculated as the sum of these five contributions.

$$C_p = C(\text{ac. translation}, 3D) + C(\text{opt. translation}, 3E) + C(\text{rotation}, 3E) + C(\text{internal}, 3E) + C_p - C_v. \quad (2)$$

Here, E and D stand for the Einstein and Debye functions, respectively. The numbers in the parentheses give the numbers of the degrees of freedom included in each term. The normal heat capacity thus calculated is given by the broken lines in Fig. 2.

The lengthy calculations involved in the optimization of the Debye and Einstein temperatures by the nonlinear least squares fitting described above were performed on a personal computer running on the BASIC. The Debye and Einstein parametrization of the vibrational heat capacity and the optimization procedure have been successfully applied to the simpler as well as more complex cases than the present one, including D_2O ice,[17] RbCN,[18] CH_3NH_3I,[19] $(CH_3NH_3)_2(TeBr_6)$,[20] $(CH_3NH_3)_2(TeI_6)$,[20] $NH_3NH_2H(CO_2)_2$,[21] and $(CD_3ND_3)_2(SnCl_6)$.[22]

No enthalpy relaxation was found in the entire temperature range. In $CsNO_2$[3,6] and $TlNO_2$[2,6] enthalpy relaxation related to the ionic reorientation occurred at low temperatures. Strong relaxational effects were also found in the dielectric measurement for these compounds. By contrast, the dielectric constant of $RbNO_2$ as a function of the temperature showed only a minor dispersion (Fig. 3). This agrees with the absence of the enthalpy relaxation in the calorimetric work.

The Enthalpy and Entropy of Transitions. The enthalpies of the transitions were determined by integrating the excess heat capacity and adding the latent heat of the transition to the integrated value. The entropies were determined in a similar way using the excess heat capacity divided by the temperature. They are collected in Table 3.

Table 3. Enthalpies and Entropies of the Phase Transitions of $RbNO_2$

T_t/K	ΔH_t/J mol^{-1}	ΔS_t/J K^{-1} mol^{-1}
83.8±0.2	48±5	0.58±0.05
264.04±0.06	9310±450	35.9±1.8

The entropy of transition determined from the high pressure phase equilibrium is 25.3 J K^{-1} mol^{-1}.[8] The previous calorimetric determination gave 32.3 J K^{-1} mol^{-1},[15] slightly smaller than the present value. The difference between the two calorimetric data may not be significant in view of the probable errors involved. The subsidiary transition at 83 K was found here for the first time and there are no other experimental data to compare with. The small entropy of transition suggests that the subsidiary transition is not an order-disorder change.

Configurational Entropy of the High-Temperature Phase. The phase equilibrium study[8] has shown that the volume change associated with the main transition is negligibly small. Therefore, it is reasonable to assume that the transition entropy is logarithmically related to the change of the number of the orientations available to the ions in the two phases.

$$\Delta S = R\ln(W_h/W_l). \quad (3)$$

Here R is the gas constant and W_h/W_l the ratio of the numbers of accessible ionic orientations in the high- and low-temperature phases, respectively. W_l may be equated to 1, because the NO_2^- ion is most probably ordered in the low-temperature phase in view of the absence of the large scale dielectric dispersion and the glass transition. The ionic disorder in the high-temperature phase is assumed to be orientational rather than positional in the sense that the positions of Rb^+ and NO_2^- ions are fixed on the fcc lattice points. We assumed further that the NO_2^- ions themselves are rigid so that they retain the C_{2v} symmetry in the crystal. Our problem is then to enumerate the allowed ionic orientations compatible with the average face-centered cubic symmetry. There is no configurational entropy for the spherically symmetric Rb^+ ion at the 4a position. The NO_2^- ion having the C_{2v} symmetry on the 4b position in the fcc Bravais lattice is obviously disordered. A nitrite group positioned about (1/2, 1/2, 1/2) is surrounded by the six nearest Rb^+ neighbours situated at the center of six faces of the cubic unit cell. The six cations form a regular octahedron. If we take the origin of the coordinate system at the center of the octahedron, the orientation of an NO_2^- ion can be specified by a set of nine position coordinates of the nitrogen and two oxygen atoms: N(a,b,c), O_I(d,e,f), and O_{II}(g,h,i). Different types of the disorder are generated by assigning one of the special or general positions to

each of the three atoms and then applying the symmetry operations to the first configuration thus specified to produce the rest.

The smallest set of the equivalent orientations has twelve members represented by

$$\begin{array}{l} \mathrm{N}\ (a,0,0) \\ \mathrm{O_I}\ (d,e,0) \\ \mathrm{O_{II}}\ (d,\bar{e},0), \end{array} \tag{4}$$

and the eleven symmetry-related orientations. An NO_2^- ion in one of these orientations has the nitrogen atom on the 4-fold axis and the ionic plane coincident with the x-y plane or its equivalent. There are two others sets of twelve members each produced from

$$\begin{array}{l} \mathrm{N}\ (a,a,0) \\ \mathrm{O_I}\ (d,e,0) \\ \mathrm{O_{II}}\ (e,d,0), \end{array} \tag{5}$$

and

$$\begin{array}{l} \mathrm{N}\ (a,a,0) \\ \mathrm{O_I}\ (d,d,f) \\ \mathrm{O_{II}}\ (d,d,\bar{f}). \end{array} \tag{6}$$

In a similar way three 24-member sets of orientations are obtained from the configurations

$$\begin{array}{l} \mathrm{N}\ (a,b,0) \\ \mathrm{O_I}\ (d,e,0) \\ \mathrm{O_{II}}\ (g,h,0), \end{array} \tag{7}$$

$$\begin{array}{l} \mathrm{N}\ (a,a,c) \\ \mathrm{O_I}\ (d,e,f) \\ \mathrm{O_{II}}\ (e,d,f), \end{array} \tag{8}$$

and

$$\begin{array}{l} \mathrm{N}\ (a,0,c) \\ \mathrm{O_I}\ (d,e,f) \\ \mathrm{O_{II}}\ (d,\bar{e},f). \end{array} \tag{9}$$

The largest set has 48 members generated from the general positions,

$$\begin{array}{l} \mathrm{N}\ (a,b,c) \\ \mathrm{O_I}\ (d,e,f) \\ \mathrm{O_{II}}\ (g,h,i). \end{array} \tag{10}$$

The entropy of the orientational disorder is $R\ln 12=20.7\ \mathrm{J\,K^{-1}\,mol^{-1}}$ for (4), (5), and (6), $R\ln 24=26.4\ \mathrm{J\,K^{-1}\,mol^{-1}}$ for (7), (8), and (9), and $R\ln 48=32.2\ \mathrm{J\,K^{-1}\,mol^{-1}}$ for (10). The experimental value is close to the last one. Therefore, the nitrite ion is disordered in the most general way in the straightforward interpretation of the experimental data. However, an additional possibility exists that there are two (or more) nonequivalent sets of low-energy configurations being nearly degenerate. If the energy difference between such sets is negligible in comparison with $RT_c\simeq 2\ \mathrm{kJ\,mol^{-1}}$, the orientations belonging to the different sets will be equally occupied in the high-temperature phase. The high-temperature entropy should then be calculated by taking the mixed configurations into account. It is equal to $R\ln(12+24)=29.8\ \mathrm{J\,K^{-1}\,mol^{-1}}$ for the combination of the orientations generated from (4) and (7) as an example. Other combinations are also possible. Therefore, more specific prediction of the disordered structure will be overly speculative at present. The conclusion drawn from the enumeration of the number of configurations is that the orientational entropy as large as $32.2\ \mathrm{J\,K^{-1}\,mol^{-1}}$ can be associated with the single ion.

A set of thirty two orientations has been proposed for a nitrite ion in KNO_2.[23] However, we could not deduce this number by the symmetry argument described here.

The large entropy of transition and the small entropy of melting are complementary with each other as often found in highly disordered molecular crystals.[24] Importance of the orientational disorder was also pointed out by Hirotsu et al. in the ultrasonic study of the cubic phase of $RbNO_2$.[25] Structural determination that may reveal the nature of the ionic disorder at the molecular level will be informative, as it was with the disordered phase of KNO_2.[23]

References

1) M. Sakiyama, A. Kimoto, and S. Seki, *J. Phys. Soc. Jpn.*, **20**, 2180 (1965).
2) K. Moriya, T. Matsuo, H. Suga, and S. Seki, *Chem. Lett.*, **1977**, 1427.
3) K. Moriya, T. Matsuo, and H. Suga, *Chem. Phys. Lett.* **82**, 581 (1981).
4) S. C. Mraw and L. A. K. Staveley, *J. Chem. Thermodyn.*, **8**, 1001 (1976).
5) S. C. Mraw, R. J. Boak, and L. A. K. Staveley, *J. Chem. Thermodyn.*, **10**, 359 (1978).
6) K. Moriya, T. Matsuo, and H. Suga, *J. Phys. Chem. Solids*, **44**, 1103 (1983).
7) K. Moriya and H. Suga, *Kagaku*, **38**, 599 (1983).
8) P. W. Richter and C. W. F. T. Pistorius, *J. Solid State Chem.*, **5**, 276 (1972).
9) B. H. Brooker and D. E. Irish, *Can. J. Chem.*, **46**, 229 (1968).
10) H. Suga and S. Seki, *Bull. Chem. Soc. Jpn.*, **38**, 1000 (1965).
11) T. Matsuo, H. Suga, and S. Seki, *J. Phys. Soc. Jpn.*, **30**, 785 (1971).
12) T. Matsuo, Y. Kume, H. Suga, and S. Seki, *J. Phys. Chem. Solids*, **37**, 499 (1976).
13) M. Oguni, T. Matsuo, H. Suga, and S. Seki, *Bull. Chem. Soc. Jpn.*, **50**, 825 (1977).
14) I. Hatta and A. Ikushima, *J. Phys. Chem. Solids*, **34**, 57 (1973).
15) R. J. Boak and L. A. K. Staveley, *J. Chem. Thermodyn.*, **19**, 661 (1987).
16) V. W. Nernst and F. A. Lindemann, *Z. Electrochem.*, **17**, 817 (1911).
17) T. Matsuo, Y. Tajima, and H. Suga, *J. Phys. Chem. Solids*, **47**, 165 (1986).

18) T. Shimada, T. Matsuo, H. Suga, and F. Luty, *J. Chem. Phys.*, **85**, 3530 (1986).
19) O. Yamamuro, M. Oguni, T. Matsuo, and H. Suga, *J. Chem. Thermodyn.*, **18**, 439 (1986).
20) N. Onoda, T. Matsuo, and H. Suga, *J. Phys. Chem. Solids*, **47**, 211 (1986).
21) T. Matsuo and H. Suga, *Thermochim. Acta*, **109**, 630 (1986).
22) T. Matsuo, H. K. Yan, and H. Suga, *J. Phys. Chem. Solids*, **49**, 85 (1988).
23) J. K. Solbakk and O. K. Strøme, *Acta Chem. Scand.*, **23**, 300 (1969).
24) N. G. Parsonage and L. A. K. Staveley, "Disorder in Crystals," Chap. 9 and 10, Clarendon Press, Oxford (1978).
25) S. Hirotsu, M. Miyamoto, and I. Yamamoto, *Jpn. J. Appl. Phys.*, **20**, L917 (1981).